HHS Public Access

Author manuscript

Curr Biol. Author manuscript; available in PMC 2017 January 11.

Published in final edited form as:

Curr Biol. 2016 January 11; 26(1): 1–13. doi:10.1016/j.cub.2015.11.020.

BLOC-1 brings together the actin and microtubule cytoskeletons to generate recycling endosomes

Cédric Delevoye[1,2,*], **Xavier Heiligenstein**[1,§], **Léa Ripoll**[1,§], **Floriane Gilles-Marsens**[1], **Megan K. Dennis**[3,4], **Ricardo A. Linares**[3,4], **Laura Derman**[1], **Avanti Gokhale**[5], **Etienne Morel**[6], **Victor Faundez**[5], **Michael S. Marks**[3,4], and **Graça Raposo**[1,2]

[1]Institut Curie, PSL Research University, CNRS, UMR144, Structure and Membrane Compartments, F-75005, Paris, France

[2]Institut Curie, PSL Research University, CNRS, UMR144, Cell and Tissue Imaging Facility (PICT-IBiSA), F-75005, Paris, France

[3]Department of Pathology and Laboratory Medicine, Children's Hospital of Philadelphia

[4]Depts. of Pathology and Laboratory Medicine and of Physiology, University of Pennsylvania, Philadelphia, PA 19104, USA

[5]Department of Cell Biology and the Center for Social Translational Neuroscience Emory University, Atlanta, Georgia 30322, USA

[6]INSERM U1151-CNRS UMR 8253, Institut Necker Enfants-Malades (INEM) Université, Paris Descartes-Sorbonne Paris Cité Paris, 75993 Paris, cedex 14, France

Summary

Recycling endosomes consist of a tubular network that emerges from vacuolar sorting endosomes and diverts cargoes toward the cell surface, the Golgi or lysosome-related organelles. How recycling tubules are formed remains unknown. We show that recycling endosome biogenesis requires the protein complex BLOC-1. Mutations in BLOC-1 subunits underlie an inherited disorder characterized by albinism, the Hermansky-Pudlak Syndrome, and are associated with schizophrenia risk. We show here that BLOC-1 coordinates the kinesin KIF13A-dependent pulling of endosomal tubules along microtubules to the Annexin A2/actin-dependent stabilization and detachment of recycling tubules. These components cooperate to extend, stabilize and form

[*]Corresponding author: Cédric Delevoye, Institut Curie, CNRS-UMR144, 26 Rue d'Ulm, 75248 Paris cedex, Tel: +33156246583; Fax: +33156246421; cedric.delevoye@curie.fr.

[§]Authors contribute equally to the work.

Supplemental Information

Supplemental Information comprises 6 Supplemental Figures, 6 Supplemental Movies, associated legends, experimental procedures and references.

Author contributions

C.D., G.R., E.M., M.S.M and V.F conceived the projects and wrote the manuscript. C.D. designed and carried out most of the experiments; X.H., L.R., F.G.M, M.K.D., R.A.L., L.D. and A.G. performed experiments; all authors edited the manuscript.

Authors declare no conflict of interest.

tubular endosomal carriers that function in cargo recycling and in the biogenesis of pigment granules in melanocytic cells. By shaping recycling endosomal tubules, our data reveal that dysfunction of the BLOC-1-KIF13A-Annexin A2 molecular network underlies the pathophysiology of neurological and pigmentary disorders.

Graphical Abstract

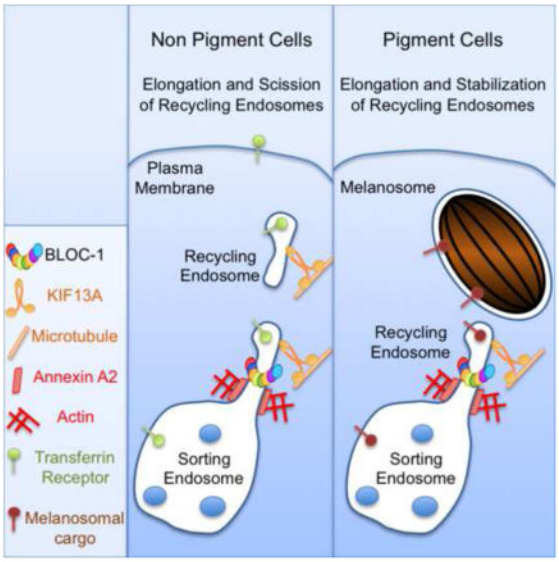

Introduction

The early endosomal system comprises a membrane network from which biosynthetic and internalized components are sorted and trafficked among multiple target compartments in all eukaryotic cells. Proper sorting and trafficking within this network is necessary to maintain cellular homeostasis and to effect ubiquitous functions (e.g. cell polarity, migration, cytokinesis and signaling) and cell type-specific functions (e.g. glucose metabolism, neurotransmitter storage and pigmentation). Transmembrane cargoes within early endosomes are sorted from vacuolar sorting endosomes (SE) or recycling endosomes (RE) [1]. REs comprise a network of interconnected and functionally distinct tubular subdomains that originate from SEs and transport their cargoes along microtubule tracks [2]. RE tubules ferry contents to the plasma membrane and the trans-Golgi-network (TGN) in all cells or to lysosome-related organelles (LROs) in specialized cell types [3, 4].

The formation and stabilization of RE tubules from SE vacuoles requires the coordination of numerous effectors [5]. Membrane curvature at SE membranes is induced and/or stabilized by cytosolic coats and associated proteins [5]. Myosin motors on membrane-associated actin filaments then generate forces necessary to elongate the necks of nascent tubules. Actin nucleators, including the ARP2/3 complex regulated by endosome-associated WASH [6] and Spire1-Annexin A2 (AnxA2) complexes [7], generate branched actin filaments on endosomes. BAR-domain-containing scaffolds such as sorting nexins stabilize curvature on newly formed RE tubules [8], but tubule elongation is likely sustained by the microtubule-

based motors, dynein and kinesins [9]. How the actin- and microtubule-associated machineries are coordinated in this process is not yet understood [5].

Specialized cell types like skin melanocytes provide a unique model for the biogenesis and function of the recycling endosomal system. Melanocytes modulate their endosomal pathway to generate melanosomes, LROs in which melanin pigments are synthesized and stored [10]. Defects in the trafficking of melanosomal cargoes (e.g. TYRP1) from endosomes to melanosomes during melanosome biogenesis underlie oculocutaneous albinism in the heritable disease, Hermansky-Pudlak Syndrome (HPS) [11]. In particular, in HPS models (HPS7, 8 and 9) that lack BLOC-1 (Biogenesis of Lysosome related Organelle Complex 1), TYRP1 and other melanosomal cargoes are trapped in enlarged SEs and fail to reach melanosome precursors [12–15], leading to impairment of pigmentation [11]. The precise role for BLOC-1 in cargo export from SEs is unknown. BLOC-1 localizes to endosomal tubules [16] and adopts a structure reminiscent of curved membrane-binding proteins [17], suggesting a potential role in stabilizing tubules.

The kinesin-3 motor, KIF13A, also facilitates the delivery of melanosomal cargoes by generating and transporting RE tubules that fuse ultimately with melanosomes [12]. Impaired KIF13A function phenocopies the hypopigmentation of BLOC-1-deficient melanocytes [12], suggesting that both may function in the same process. Moreover, genetic variations in KIF13A or BLOC-1 subunits appear to predispose to neurological disorders like schizophrenia [18–20].

Here we show that BLOC-1 coordinates the action of microtubule- and actin-dependent machineries to elongate, stabilize and ultimately release RE tubules. The molecular linkage between actin and microtubule cytoskeletons by BLOC-1 explains the molecular defect in HPS.

Results

BLOC-1 is required for recycling endosome tubule biogenesis

The eight-subunit BLOC-1 is destabilized by loss of expression of the Pallidin, Muted or Snapin subunits [21–23]. We investigated whether BLOC-1 supports RE tubule formation by quantifying KIF13A-positive ($KIF13A^+$) endosomal tubules in HeLa cells treated with a collection of siRNAs to these subunits (BLOC-1 siRNA), which effectively reduced expression of Pallidin, Muted and the non-siRNA-targeted Dysbindin subunits relative to a control siRNA (Figure 1A). By live fluorescence imaging of HeLa cells treated with control siRNA, KIF13A-YFP (KIF13A) was detected in long RE tubules (arrows) that extended toward the cell periphery and were labeled by internalized transferrin-Alexafluor546 conjugates (TfA546; Figures 1B, S1A–B, Movie S1 and [24]). In contrast, BLOC-1-depleted cells accumulated KIF13A in enlarged, round and mostly static $TfA546^+$ endocytic structures that were devoid of tubules (Figures 1B, S1C–F, arrowheads; Movie S2). Discrete $KIF13A^+$ and $TfA546^+$ structures emanated from these endosomes but did not elongate or detach over 1 min (Figures S1D, S1F, Movie S3). A small fraction of $KIF13A^+$ tubules (likely the least dynamic population) was stable to chemical fixation; by immunofluorescence microscopy (IFM), the percentage of cells that harbored at least one

such KIF13A$^+$ tubule was ~40% reduced in BLOC-1-depleted cells relative to controls (Figure 1C). This likely underestimated the defect in these cells, since most KIF13A$^+$ tubules — as described generally for early endosomal tubules [25] — are sensitive to aldehyde fixation [24]. Indeed, by live cell microscopy analysis (Figures 1D–E), the average number of dynamic KIF13A$^+$ tubules was dramatically decreased by BLOC-1-depletion. Moreover the detected tubules were significantly shorter (Figure 1F), indicating a defect in RE tubule elongation. Whereas KIF13A segregated from SE in control cells and thus did not colocalize with SE-associated RAB5 (arrowheads), KIF13A co-distributed with RAB5$^+$ and Tf$^+$ SEs in BLOC-1-depleted cells (Figure 1G, arrows). This result supports our earlier data that RE tubules emerge from SE vacuolar domains in melanocytes [12, 26], and indicates that the primary source of KIF13A$^+$ RE membranes are RAB5$^+$ SEs. Moreover, as in siKIF13A-treated cells [24], Tf recycling was consistently reduced after 40 min of chase in BLOC-1-depleted cells relative to controls (Figure S1G). These observations suggest that BLOC-1 acts upstream of KIF13A during RE tubule biogenesis from SE in HeLa cells.

BLOC-1 promotes elongation of nascent recycling endosomal tubules

To better define the organelles from which RE tubules emanate and how they are controlled by BLOC-1, we analyzed cells by correlative light and electron microscopy (CLEM). KIF13A-YFP-expressing, BLOC-1-depleted HeLa cells that had internalized TfA546 were immobilized by high pressure freezing (HPF) and processed for EM (Experimental Procedures and [27]). Consecutive sections of 250 and 70 nm in thickness were analyzed. The thick section was screened by FM for cells harboring large TfA546$^+$ and KIF13A$^+$ structures (Figures 2A, S2A; arrows) that accumulate upon BLOC-1-depletion (Figure 1B). Identified structures were tracked on the thin section (Figures 2B, S2B; arrows) on which FM and EM images were acquired and overlaid (Figures 2C, S2C). KIF13A$^+$ and TfA546$^+$ structures had morphological features of SEs — vacuolar structures (~400 nm in diameter) containing none or few intraluminal vesicles (ILVs) (Figures 2D–E, S2D). These SEs harbored multiple short budding profiles (Figures 2D–E, S2D, Movie S4; arrowheads and schematized in Figure 2F), sometimes associated with tubular necks (Figures 2D, S2D; arrows) that were devoid of an apparent clathrin coat, reflecting local deformations of the SE membrane. By contrast (Figure 1B), KIF13A and internalized Tf co-distributed to the periphery of siCTRL-treated cells by FM (Figures S2E–G, arrows); these areas corresponded by EM to regions enriched in tubules and vesicles (≤ 100 nm in diameter) characteristic of REs (Figure S2H, boxes 1–3, arrowheads; and [2]). Importantly, very few budding profiles were observed on SEs in siCTRL cells (Figure S2H, boxes 2 and 4; arrows and Figure S2I, arrowheads) showing that they accumulated only upon BLOC-1 depletion (Figures 2, S2).

We evaluated the number and shape of budded structures on endosomes in CTRL- and BLOC-1-depleted cells investigated by CLEM. BLOC-1 depletion increased 3-fold the number of round buds on endosomes (Figures 2E, 2G, arrowheads) but did not affect the number of elongated budded structures (Figure 2D, box 1, arrow and Figure 2G) or the shape of the round buds (Figures 2E, 2H, arrowheads). If BLOC-1 were to promote bud formation by bending the SE limiting membrane or to promote RE tubule detachment, BLOC-1 depletion would either reduce the number of round buds or increase elongated

buds, respectively. By contrast, the accumulation of round buds (Figure 2) and loss of tubules (Figure 1) suggests that those buds can neither elongate nor detach from the SE limiting membrane. We thus conclude that BLOC-1 promotes the extension and maturation of round buds into recycling tubular carriers, and may contribute later to their stabilization. Such a role for BLOC-1 in stabilizing elongated buds would be consistent with its curvilinear structure [17] and its localization to endocytic tubules [16].

BLOC-1 controls endosomal tubule formation in melanocytes

As BLOC-1 and KIF13A are required in melanocytes to deliver newly synthesized melanogenic cargoes from SEs to maturing melanosomes [13–16, 28], and BLOC-1-deficient [14] or KIF13A-depleted melanocytes [12] accumulate enlarged vacuolar endosomes in which these cargoes are retained, we tested whether BLOC-1 controls RE tubule generation in melanocytes. REs labeled by transfected GFP-tagged syntaxin 13 (STX13) [29], as previously described [26], were detected by live cell imaging in BLOC-1-deficient (BLOC-$1^{-/-}$) melanocytes (melan-pa) derived from *pallid* mice or "rescued" melan-pa cells (BLOC-1^{R}) expressing the missing Pallidin subunit [14]. In BLOC-1^{R} melanocytes, STX13 labeled numerous cytoplasmic puncta and long tubules (Figures 3A–B, arrows). By contrast, STX13-labeled tubules were barely detected in BLOC-$1^{-/-}$ cells (Figure 3A, bottom panel, arrows), and those detected were significantly shorter than in BLOC-1^{R} cells (Figures 3A–B). Rather, BLOC-$1^{-/-}$ cells harbored enlarged and clustered STX13-labeled vacuoles (Figure 3A, arrowheads) similar to the SE vacuoles detected previously by EM [14]. These data indicate that BLOC-1 is required for the elongation of RE tubules out of SEs in different cell types.

BLOC-1 cooperates with KIF13A in melanosome biogenesis

To test whether BLOC-1 and KIF13A cooperate within the same endosome-melanosome cargo transport pathways, we compared pigmentation and melanosome biogenesis in human MNT-1 melanocytic cells depleted of BLOC-1 or KIF13A alone or together. Cells treated with CTRL-, BLOC-1-, KIF13A- or BLOC-1 and KIF13A siRNAs resulted in specific depletion of KIF13A and/or BLOC-1 subunits (Figure 3C). By conventional EM, single depletion of either BLOC-1 or KIF13A caused a loss of mature pigmented stage III and IV melanosomes relative to controls (Figures S3A–B, 3D; arrows) and a concomitant increase in immature and unpigmented stage I and II melanosomes (arrowheads), indicating a block in melanosome maturation as previously shown [12, 14]. Depletion of both BLOC-1 and KIF13A yielded an identical phenotype (Figure 3D) and a similar proportion of immature to mature melanosomes (Figure 3E). Accordingly, depletion of either BLOC-1, KIF13A or both decreased the intracellular melanin content by ~30% from control values (Figure 3F). The lack of a synergistic effect on either melanosome maturation or pigmentation suggests that BLOC-1 and KIF13A cooperate in the same cargo transport pathway.

We then tested whether BLOC-1 interacted physically with KIF13A. Whereas the endogenous BLOC-1 subunits Pallidin and Dysbindin were not enriched in anti-GFP immunoprecipitates (IP) of HeLa cells expressing either GFP or YFP-KIF5B as controls, they were detected in IP of cells expressing a GFP-tagged motor-deleted form of KIF13A

(GFP-KIF13A-ST) (Figures 3G, S3C) that localizes to endosomes [24]. These data suggest that BLOC-1 and KIF13A associate within cells.

ARP2/3-dependent actin polymerization stabilizes recycling endosomal tubules

Because actin polymerization can participate in the elongation, stabilization and/or fission of endosomal membranes [5], we investigated the role of actin dynamics in generating KIF13A driven-RE tubules. Brief incubation of KIF13A-expressing HeLa cells with the F-actin depolymerizing agent Latrunculin A (LatA) depleted actin fibers labeled by phalloidin-A546 (Figure 4A) and decreased by IFM the frequency of cells harboring at least one KIF13A RE tubule by ~25% relative to DMSO-treated cells (Figures 4A–B). LatA-treatment showed a more dramatic reduction in dynamic tubule number and length (Figures 4C–E), comparable to BLOC-1-depletion (Figures 1E–F), when analyzed by live cell imaging. In LatA-treated cells, KIF13A associated with enlarged (Figure 4A, arrows) and largely immobile (Movie S5) Tf^{+} structures resembling those in BLOC-1-depleted cells (Figures 1B, S1C–F). Addition of LatA 5 min before video microscopy analysis revealed rapid retraction and collapse of KIF13A-containing tubules (Movie S5), showing that actin dynamics are required for optimal microtubule-dependent elongation of RE tubules [24].

To define the machinery that promotes actin polymerization during RE tubule formation, HeLa cells were analyzed after treatment with inhibitors of the ARP2/3 complex (CK-666) or formin family proteins (SMIFH2). Relative to vehicle (DMSO), CK-666, but not SMIFH2, reduced the frequency of cells with at least one KIF13A-RE tubule by ~25 % by IFM (Figures 4B, 4F) — as much as LatA treatment — and dramatically decreased the number and length of dynamic $KIF13A^{+}$ tubules by live cell imaging (Figures 4C–E). As with LatA, CK-666-treated cells harbored enlarged $KIF13A^{+}$ structures despite no general effect on actin fibers (Figure 4F, top panels, arrows). In contrast, SMIFH2-treated cells still generated KIF13A-labeled tubules (Figure 4F, bottom panels, arrows) that were transported towards the cell periphery (arrowheads) like in control cells (Figures 4A, 4C, top panels). Peripheral KIF13A-containing puncta that were observed in control cells by IFM and live imaging (Figures 4A, 4C, arrowheads and [24]) were abolished by combined treatment with nocodazole and LatA or CK-666, then restored upon washout of all drugs but not upon washout of the actin drugs alone (Figure 4G). This shows that ARP2/3-dependent actin polymerization alone, in the absence of microtubules, is not sufficient to elongate RE tubules. Our data together show that ARP2/3-dependent but formin-independent actin polymerization is required for the stabilization of KIF13A-RE tubules.

ARP2/3-dependent actin polymerization requires activation. The WASH complex activates ARP2/3 on endosomes [6] following its recruitment by retromer [30], but our data do not support a role for WASH in KIF13A-dependent RE tubule formation. First, whereas KIF13A co-distributed by IFM with AP-1 [12] or internalized Tf [24] (arrows), it did not co-localize significantly with WASH or the VPS35 subunit of retromer (arrowheads) (Figure S4A). Second, siRNA depletion of WASH or the retromer subunit VPS35 in KIF13A-expressing cells did not affect the generation of KIF13A-RE tubules (Figures S4B–D, arrows). Third, WASH depletion in melanocytic cells did not impair pigmentation like KIF13A or BLOC-1 depletion (Figure S4E; compare to Figure 3F), indicating that WASH is

not required for melanosome maturation. Thus, RE tubule stabilization and/or fission requires the ARP2/3-dependent but WASH-independent local polymerization of branched actin filaments, likely on SE membranes.

Annexin A2 is required to generate recycling endosomal tubules

We next tested whether Annexin A2 (AnxA2) serves as an alternative to WASH in ARP2/3 activation during RE tubule formation. AnxA2 is a phospholipid binding protein [31] that initiates ARP2/3-dependent actin polymerization on early endosomal membranes [7]. Consistent with the detection of AnxA2 on endosomal tubules [32, 33], endogenous AnxA2 decorated KIF13A$^+$ tubules in HeLa cells (Figures 5A–B, arrows). Endogenous AnxA2 was co-immunoprecipitated with GFP-KIF13A-ST or GFP-KIF13A-T (containing only the KIF13A tail domain; [12]), but not with GFP alone, the melanosome-associated myosin VI motor [34], or the kinesin-1 KIF5B (Figures 5C, S5A–B), indicating that AnxA2 associated physically with the KIF13A tail.

We then tested whether AnxA2 modulates RE function. In agreement with previous reports [35, 36], AnxA2 depletion by siRNA (Figure 5D) impaired Tf recycling as shown by higher intracellular Tf intensity after 40 min of chase relative to controls (Figure S5C). Moreover, as for BLOC-1 depletion or Arp2/3 inhibition, ~20% fewer AnxA2-depleted cells harbored at least one KIF13A-RE tubule relative to controls (Figure 5E), the number and length of dynamic tubules by live cell imaging was dramatically reduced (Figures 5F–G), and KIF13A accumulated on enlarged Tf$^+$ and Rab5$^+$ SEs (Figures 5H, S5D; arrowheads). Thus, AnxA2 activity facilitates the generation of KIF13A-dependent RE tubules from SEs.

To characterize the effects of AnxA2 depletion on endosome morphology, AnxA2-depleted cells expressing KIF13A-YFP were analyzed by HPF-CLEM following TfA546 internalization. Cells harboring large KIF13A$^+$ (green) and Tf$^+$ (red) structures were identified by FM on 250 nm thick sections (Figure S5E, arrows), and the corresponding 70 nm thin sections were used for correlative image registration (Figures S5F, 5I; arrows). Like in BLOC-1-depleted cells but not control cells (Figures 2, S2), fluorescent structures in AnxA2-depleted cells corresponded to SEs containing ILVs from which several buds emanated (Figures 5J, S5G, Movie S6; arrowheads). Endosomes harbored slightly more rounded buds than controls, but most buds were elongated compared to those in CTRL- or BLOC-1-depleted cells (Figures 5J–L, S5G, Movie S6; arrows). These tubular structures — defined as elongated buds — remained attached to the SE limiting membrane and increased 8-fold relative to either CTRL- (Figures 5J, 5L; arrows) or BLOC-1-depleted cells (Figure 2G). These data suggest that AnxA2 functions downstream of BLOC-1 in the stabilization and/or scission of KIF13A-dependent RE tubules from the limiting membrane of SEs.

Annexin A2 cooperates with BLOC-1 on endosomes

Although they cooperate functionally with KIF13A activity at the SE, attempts to demonstrate a physical association between AnxA2 and BLOC-1 were unsuccessful (data not shown). However, by IFM on siBLOC-1-treated HeLa cells, a cohort of AnxA2 co-distributed with KIF13A in Tf-containing endosomes (Figure 6A, arrows) rather than on RE tubules as in controls (Figure 5A, arrows). These endosomes likely corresponded to the SEs

identified by CLEM in BLOC-1-depleted cells (Figures 2D–E, S2D), indicating that BLOC-1 is not required to recruit AnxA2 to SEs. IFM and IEM analyses showed that endosomes in BLOC-1-inactivated cells were depleted of actin fibers (Figures S6A–C, arrows), indicating that the AnxA2 accumulated on these endosomes do not hyper-stimulate actin polymerization. Interestingly, the fraction of AnxA2 co-immunoprecipitated by KIF13A decreased in siBLOC-1-treated cells relative to controls (Figure 6B), suggesting that BLOC-1 stabilizes the interaction between KIF13A and AnxA2 and might promote the local association of AnxA2 with emanating REs. Additionally and like other BLOC-1 interacting proteins [37], long term Pallidin shRNA treatment (Figures S6D–E, 7 days) – but not short term siBLOC-1 depletion (Figure 6C, lane 2; ~3 days) – reduced AnxA2 expression relative to controls, suggesting that BLOC-1 might also stabilize AnxA2. Thus, BLOC-1 functions upstream of AnxA2 with which it cooperates to control the elongation and/or scission of KIF13A$^+$ RE tubules from SEs.

Annexin A2 cooperates with BLOC-1 and KIF13A in melanosome biogenesis

Since AnxA2 promotes BLOC-1- and KIF13A-dependent RE tubule formation in HeLa cells and similar RE tubules function in melanosome biogenesis in melanocytes, we addressed whether AnxA2 controls melanosome maturation. Relative to that of controls, the melanin content of AnxA2-depleted melanocytes was reduced by ~20% (Figures 6C–D, lane 4), as observed in BLOC-1- or KIF13A-inactivated cells (Figures 6C–D). Concomitant depletion of AnxA2 and either BLOC-1, KIF13A or both did not further reduce pigmentation relative to cells depleted singly of BLOC-1 or KIF13A (Figures 6C–D), suggesting that AnxA2, BLOC-1 and KIF13A function within the same endosome-to-melanosome pathway. AnxA2-depleted melanocytes, like those depleted of BLOC-1 or KIF13A (Figures 3D–E, S3A–B), had drastically fewer pigmented melanosomes than controls (arrows) and accumulated immature non-pigmented melanosomes (arrowheads) (Figures 6E–F). Thus, AnxA2 promotes melanosome maturation and pigmentation. The lack of additive effects with KIF13A and/or BLOC-1 depletion and the similarity of the phenotypes lead us to propose that AnxA2 cooperates with BLOC-1 and KIF13A to regulate the formation of tubular RE transport intermediates that function in melanosome biogenesis.

Discussion

Recycling endosomes were identified three decades ago [2], but the molecular mechanisms underlying their formation remain poorly understood, likely owing to the functional redundancy of endosomal domains that can support the recycling of most studied cargoes [38]. Here we detail key players in RE biogenesis by exploiting two functional readouts: the tubular morphology of REs in HeLa cells and RE-dependent melanosome maturation in melanocytic cells. Our results identify BLOC-1, a schizophrenia susceptibility factor and the target of mutation in HPS subtypes, as an endocytic module linking microtubule (KIF13A) and actin (Annexin A2) cytoskeleton-related machineries to couple the remodeling of SE membranes to the generation, elongation and scission of RE tubules.

RE tubule biogenesis starts with the generation of membrane curvature on SE membranes. Local membrane deformation can recruit membrane sensors, like BAR domain-containing

proteins, that might stabilize and/or elongate nascent tubules. BLOC-1 might function as such a sensor for nascent RE tubules, since recombinant BLOC-1 forms a curvilinear chain with a substantial bend by negative stain electron microscopy [17] and localizes to tubular endosomes by whole mount EM [16]. Accordingly, the increased number of buds associated to endosomes in BLOC-1-depleted cells indicates that BLOC-1 functions downstream of the first remodeling event. We therefore propose that BLOC-1 is preferentially recruited to nascent RE buds where it functions as a molecular scaffold for further elongation of the RE tubule. The interaction of BLOC-1 with KIF13A — the first microtubule-associated motor identified to interact functionally and physically with BLOC-1 — might then permit KIF13A to engage microtubules to initiate tubule elongation. The interaction of BLOC-1 with KIF13A mirrors the indirect association of the related BORC with Kinesin-1 to regulate motility of lysosomes [39], and might reflect an evolutionary conserved function of the common BLOC-1 and BORC subunits. Interestingly, we also observed interactions of KIF17 with BLOC-1 and AnxA2 (our unpublished observations). KIF17 promotes cargo trafficking [40] to actin-rich synaptic regions in post-synaptic neurons [41]. One may speculate that the BLOC-1/AnxA2 module may engage other kinesins for additional broader functions.

The bending and elongation of the SE membrane must be supported and sustained by actin-driven mechanical forces, as proposed during endocytosis [42, 43]. We demonstrate that BLOC-1 cooperates with AnxA2 and Arp2/3 to stabilize RE tubules in HeLa cells and melanocytes. By favoring the interaction of AnxA2 with KIF13A, BLOC-1 functions upstream of both the microtubule- and actin-dependent machineries in the elongation and stabilization of nascent RE tubules. Whereas BLOC-1 engages actin regulators such as WASH [21, 37, 44] in some cell types and WASH controls the trafficking of some BLOC-1-dependent cargoes [37], we show that BLOC-1 and WASH play distinct roles in RE tubule generation and melanosome biogenesis. The cooperation between BLOC-1 and WASH is likely dependent on cell type, endosomal subpopulation and/or cargo.

BLOC-1 functions in RE biogenesis through AnxA2 to activate Arp2/3 to initiate branched actin filaments [7]. AnxA2 associates to early endosomes [32] and modulates endosomal dynamics and function along recycling [35, 36] and degradative pathways [45, 46]. AnxA2 depletion has also been shown to block early to late endosome maturation without affecting ILV formation [45]. Similar defects were observed upon KIF13A or BLOC-1 depletion [24, 47], whereas selected cargo sorting of PMEL to ILVs was unaffected [12, 14]. These data suggest that AnxA2, BLOC-1 and KIF13A cooperate to regulate early to late endosome maturation. This is likely a consequence of their effects on RE tubule formation, as vacuolar SE and tubular RE are interconnected subdomains; therefore, impairing the formation of RE tubules would prevent SE limiting membrane remodeling required for proper cargo sorting and endosome maturation [12, 24].

By linking actin and microtubule machineries, BLOC-1 is well suited to orchestrate the elongation and detachment of RE tubules from SE and thus to effect the sorting of cargoes destined for LROs in cells like melanocytes or for the plasma membrane or Golgi in other cell types. We propose a model of RE tubule biogenesis (Figure 6G) that incorporates our findings. First, membrane deformation of the flat SE membrane (**1**) generates a curved bud

to which BLOC-1 associates (**2**). This facilitates KIF13A recruitment to SE subdomains (**3**), which promotes bud elongation along microtubules (**4**). Then, AnxA2 activates ARP2/3-dependent local polymerization of branched actin filaments (**5**) [7], stabilizing and allowing for the potential scission of the newly formed RE tubule. The tubule is then transported along the microtubule network towards its destination — the plasma membrane [24] or maturing melanosomes [12] — via KIF13A. In this model, KIF13A motor activity along microtubules generates the pulling force required to sustain tubule elongation (**4**), whereas AnxA2 and actin polymerization likely participate in the scission of the RE intermediates from SEs in HeLa cells (**5**) or in RE tubule stabilization in melanocytes where RE intermediates are stably connected to SEs [12, 26]. BLOC-1 bridges the gap between the tubular membrane and microtubules via its interaction with KIF13A and between the two cytoskeletons by stabilizing AnxA2-KIF13A complexes.

Despite the ubiquitous expression of BLOC-1, disruption of BLOC-1 function only manifests with overt phenotypes in a subset of cell types like melanocytes, platelets and neurons. This reflects the non-redundant function of BLOC-1 in the trafficking of specific cargoes, such as TYRP1, OCA2 and ATP7A in melanocytes [13–15] or dopamine receptor and synaptic vesicle proteins in neurons [48]. Patients or related mouse models of HPS types 7–9 harboring BLOC-1 mutations suffer from albinism and excessive bleeding [11] and are associated with increased risk of schizophrenia [48]. *KIF13A* is a candidate gene for schizophrenia [18], and *Kif13a*$^{-/-}$ mice develop a neurological disorder reflected by elevated anxiety [20]. Our study suggests that the function of the AnxA2-BLOC-1-KIF13A network in shaping RE membrane tubules is a common underlying basis for the pigmentary and neurological defects observed in this disorder.

Experimental Procedures

Statistical Analysis

Unless specified, statistical differences were evaluated between means taken in pairs by Student's *t* test adapted for small number of samples. A *P*-value <0.05 was considered as statistically significant.

Correlative Light and Electron Microscopy

HeLa cells cultured 48h in CryoCapsules® [27] were treated with CTRL-, BLOC1- or AnxA2-siRNAs (48h) and transfected with KIF3A-YFP encoding plasmids (20h). TfA546 uptake was performed 1h prior to high pressure freezing (HPM100, Leica microsystem), then cells were freeze substituted (12h) with 0.05% uranyl acetate, 0.01% gluraldehyde and 1% H_2O in dry acetone and embedded in Lowicryl to preserve the fluorescence in bloc. After CryoCapsules® removal from the polymerized Lowicryl bloc [49], cells were sectioned with one 250 nm section followed by two or three 70 nm sections. The 250 nm sections were collected on a glass coverslip, mounted with Hoechst-containing mowiol in PBS medium and imaged (Te2000 epifluorescence microscope). The 70 nm sections were collected on slot grids, floated on Hoechst solution (20 min), rinsed in distilled H_2O and stored in dark environment. The fluorescent signal on 70 nm sections is comparable to confocal sections due to the physical thickness of the section allowing accurate

identification and imaging of cells. The nucleus shape was used to improve cell re-location and fluorescent image postprocessing was performed to increase the signal to noise ratio prior to correlative image registration. The 70 nm sections were post-stained with lead citrate (5 min) and imaged (Tecnai Spirit G2; FEI) at increasing magnifications (2500x to 15000x).

Supplementary Material

Refer to Web version on PubMed Central for supplementary material.

Acknowledgments

We are grateful to S. Miserey-Lenkei, JB. Brault, P. Monteiro, P. Chavrier and H. Racine (Institut Curie), E. Dell'Angelica (University of California, USA), A. Gautreau (Gif-sur-Yvette, France), V. Gerke (University of Muenster, Germany) and LY. Jan (UCSF, HHMI, USA) for generous gifts of reagents; G. van Niel and C. Bissig for insightful discussions; R. Basto for critical reading of the manuscript; L. Sengmanivong and V. Fraisier (Spatio Temporal Modeling Imaging and Cellular Dynamics-Institut Curie) for image acquisition and deconvolution; and J. Burkhardt (Children's Hospital of Philadelphia, PA, USA) for using confocal microscope for image acquisition with mouse melanocytes. The authors greatly acknowledge the Nikon Imaging Center @ Institut Curie-CNRS, and the PICT-IBiSA, member of the France-BioImaging national research infrastructure, supported by the CelTisPhyBio Labex (N° ANR-10-LBX-0038) part of the IDEX PSL (N° ANR-10-IDEX-0001-02 PSL). This work was supported by CNRS, INSERM, Institut Curie, National Institutes of Health grants (GM077569 and NS088503 to V.F.), R01 EY015625 from the National Eye Institute (to M.S.M. and G.R.), R01 AR048155 from NIAMS (to M.S.M.) and F32 AR062476 (to M.K.D), and Fondation pour la Recherche Médicale (FRM grant DEQ20140329491 Team label to G.R.).

References

1. Klumperman J, Raposo G. The Complex Ultrastructure of the Endolysosomal System. Cold Spring Harb Perspect Biol. 2014
2. Willingham MC, Hanover JA, Dickson RB, Pastan I. Morphologic characterization of the pathway of transferrin endocytosis and recycling in human KB cells. Proc Natl Acad Sci U S A. 1984; 81:175–179. [PubMed: 6141558]
3. Grant BD, Donaldson JG. Pathways and mechanisms of endocytic recycling. Nature reviews Molecular cell biology. 2009; 10:597–608. [PubMed: 19696797]
4. Marks MS, Heijnen HF, Raposo G. Lysosome-related organelles: unusual compartments become mainstream. Current opinion in cell biology. 2013; 25:495–505. [PubMed: 23726022]
5. Anitei M, Hoflack B. Bridging membrane and cytoskeleton dynamics in the secretory and endocytic pathways. Nat Cell Biol. 2012; 14:11–19. [PubMed: 22193159]
6. Derivery E, Sousa C, Gautier JJ, Lombard B, Loew D, Gautreau A. The Arp2/3 activator WASH controls the fission of endosomes through a large multiprotein complex. Dev Cell. 2009; 17:712–723. [PubMed: 19922875]
7. Morel E, Parton RG, Gruenberg J. Annexin A2-dependent polymerization of actin mediates endosome biogenesis. Dev Cell. 2009; 16:445–457. [PubMed: 19289089]
8. Mim C, Unger VM. Membrane curvature and its generation by BAR proteins. Trends Biochem Sci. 2012; 37:526–533. [PubMed: 23058040]
9. Granger E, McNee G, Allan V, Woodman P. The role of the cytoskeleton and molecular motors in endosomal dynamics. Semin Cell Dev Biol. 2014; 31:20–29. [PubMed: 24727350]
10. Raposo G, Marks MS. Melanosomes--dark organelles enlighten endosomal membrane transport. Nature reviews Molecular cell biology. 2007; 8:786–797. [PubMed: 17878918]
11. Wei AH, Li W. Hermansky-Pudlak syndrome: pigmentary and non-pigmentary defects and their pathogenesis. Pigment Cell Melanoma Res. 2013; 26:176–192. [PubMed: 23171219]
12. Delevoye C, Hurbain I, Tenza D, Sibarita JB, Uzan-Gafsou S, Ohno H, Geerts WJ, Verkleij AJ, Salamero J, Marks MS, et al. AP-1 and KIF13A coordinate endosomal sorting and positioning

during melanosome biogenesis. The Journal of cell biology. 2009; 187:247–264. [PubMed: 19841138]

13. Setty SR, Tenza D, Sviderskaya EV, Bennett DC, Raposo G, Marks MS. Cell-specific ATP7A transport sustains copper-dependent tyrosinase activity in melanosomes. Nature. 2008; 454:1142–1146. [PubMed: 18650808]
14. Setty SR, Tenza D, Truschel ST, Chou E, Sviderskaya EV, Theos AC, Lamoreux ML, Di Pietro SM, Starcevic M, Bennett DC, et al. BLOC-1 is required for cargo-specific sorting from vacuolar early endosomes toward lysosome-related organelles. Molecular biology of the cell. 2007; 18:768–780. [PubMed: 17182842]
15. Sitaram A, Dennis MK, Chaudhuri R, De Jesus-Rojas W, Tenza D, Setty SR, Wood CS, Sviderskaya EV, Bennett DC, Raposo G, et al. Differential recognition of a dileucine-based sorting signal by AP-1 and AP-3 reveals a requirement for both BLOC-1 and AP-3 in delivery of OCA2 to melanosomes. Molecular biology of the cell. 2012; 23:3178–3192. [PubMed: 22718909]
16. Di Pietro SM, Falcon-Perez JM, Tenza D, Setty SR, Marks MS, Raposo G, Dell'Angelica EC. BLOC-1 interacts with BLOC-2 and the AP-3 complex to facilitate protein trafficking on endosomes. Molecular biology of the cell. 2006; 17:4027–4038. [PubMed: 16837549]
17. Lee HH, Nemecek D, Schindler C, Smith WJ, Ghirlando R, Steven AC, Bonifacino JS, Hurley JH. Assembly and architecture of biogenesis of lysosome-related organelles complex-1 (BLOC-1). The Journal of biological chemistry. 2012; 287:5882–5890. [PubMed: 22203680]
18. Jamain S, Quach H, Fellous M, Bourgeron T. Identification of the human KIF13A gene homologous to Drosophila kinesin-73 and candidate for schizophrenia. Genomics. 2001; 74:36–44. [PubMed: 11374900]
19. Mullin AP, Gokhale A, Larimore J, Faundez V. Cell biology of the BLOC-1 complex subunit dysbindin, a schizophrenia susceptibility gene. Mol Neurobiol. 2011; 44:53–64. [PubMed: 21520000]
20. Zhou R, Niwa S, Guillaud L, Tong Y, Hirokawa N. A molecular motor, KIF13A, controls anxiety by transporting the serotonin type 1A receptor. Cell Rep. 2013; 3:509–519. [PubMed: 23438369]
21. Falcon-Perez JM, Starcevic M, Gautam R, Dell'Angelica EC. BLOC-1, a novel complex containing the pallidin and muted proteins involved in the biogenesis of melanosomes and platelet-dense granules. The Journal of biological chemistry. 2002; 277:28191–28199. [PubMed: 12019270]
22. Li W, Zhang Q, Oiso N, Novak EK, Gautam R, O'Brien EP, Tinsley CL, Blake DJ, Spritz RA, Copeland NG, et al. Hermansky-Pudlak syndrome type 7 (HPS-7) results from mutant dysbindin, a member of the biogenesis of lysosome-related organelles complex 1 (BLOC-1). Nature genetics. 2003; 35:84–89. [PubMed: 12923531]
23. Starcevic M, Dell'Angelica EC. Identification of snapin and three novel proteins (BLOS1, BLOS2, and BLOS3/reduced pigmentation) as subunits of biogenesis of lysosome-related organelles complex-1 (BLOC-1). J Biol Chem. 2004; 279:28393–28401. [PubMed: 15102850]
24. Delevoye C, Miserey-Lenkei S, Montagnac G, Gilles-Marsens F, Paul-Gilloteaux P, Giordano F, Waharte F, Marks MS, Goud B, Raposo G. Recycling endosome tubule morphogenesis from sorting endosomes requires the kinesin motor KIF13A. Cell Rep. 2014; 6:445–454. [PubMed: 24462287]
25. Murk JL, Posthuma G, Koster AJ, Geuze HJ, Verkleij AJ, Kleijmeer MJ, Humbel BM. Influence of aldehyde fixation on the morphology of endosomes and lysosomes: quantitative analysis and electron tomography. J Microsc. 2003; 212:81–90. [PubMed: 14516365]
26. Dennis MK, Mantegazza AR, Snir OL, Tenza D, Acosta-Ruiz A, Delevoye C, Zorger R, Sitaram A, de Jesus-Rojas W, Ravichandran K, et al. BLOC-2 targets recycling endosomal tubules to melanosomes for cargo delivery. The Journal of Cell Biology. 2015; 209:563–577. [PubMed: 26008744]
27. Heiligenstein X, Heiligenstein J, Delevoye C, Hurbain I, Bardin S, Paul-Gilloteaux P, Sengmanivong L, Regnier G, Salamero J, Antony C, et al. The CryoCapsule: simplifying correlative light to electron microscopy. Traffic. 2014; 15:700–716. [PubMed: 24533564]

28. Cullinane AR, Curry JA, Carmona-Rivera C, Summers CG, Ciccone C, Cardillo ND, Dorward H, Hess RA, White JG, Adams D, et al. A BLOC-1 mutation screen reveals that PLDN is mutated in Hermansky-Pudlak Syndrome type 9. Am J Hum Genet. 2011; 88:778–787. [PubMed: 21665000]
29. Prekeris R, Klumperman J, Chen YA, Scheller RH. Syntaxin 13 mediates cycling of plasma membrane proteins via tubulovesicular recycling endosomes. J Cell Biol. 1998; 143:957–971. [PubMed: 9817754]
30. Harbour ME, Breusegem SY, Seaman MN. Recruitment of the endosomal WASH complex is mediated by the extended 'tail' of Fam21 binding to the retromer protein Vps35. The Biochemical journal. 2012; 442:209–220. [PubMed: 22070227]
31. Gerke V, Creutz CE, Moss SE. Annexins: linking Ca2+ signalling to membrane dynamics. Nature reviews Molecular cell biology. 2005; 6:449–461. [PubMed: 15928709]
32. Emans N, Gorvel JP, Walter C, Gerke V, Kellner R, Griffiths G, Gruenberg J. Annexin II is a major component of fusogenic endosomal vesicles. The Journal of cell biology. 1993; 120:1357–1369. [PubMed: 8449982]
33. Zeuschner D, Stoorvogel W, Gerke V. Association of annexin 2 with recycling endosomes requires either calcium- or cholesterol-stabilized membrane domains. Eur J Cell Biol. 2001; 80:499–507. [PubMed: 11561901]
34. Loubery S, Delevoye C, Louvard D, Raposo G, Coudrier E. Myosin VI regulates actin dynamics and melanosome biogenesis. Traffic. 2012; 13:665–680. [PubMed: 22321127]
35. Moreau K, Ghislat G, Hochfeld W, Renna M, Zavodszky E, Runwal G, Puri C, Lee S, Siddiqi F, Menzies FM, et al. Transcriptional regulation of Annexin A2 promotes starvation-induced autophagy. Nat Commun. 2015; 6:8045. [PubMed: 26289944]
36. Zobiack N, Rescher U, Ludwig C, Zeuschner D, Gerke V. The annexin 2/S100A10 complex controls the distribution of transferrin receptor-containing recycling endosomes. Molecular biology of the cell. 2003; 14:4896–4908. [PubMed: 13679511]
37. Ryder PV, Vistein R, Gokhale A, Seaman MN, Puthenveedu M, Faundez V. The WASH Complex, an Endosomal Arp2/3 Activator, Interacts with the Hermansky-Pudlak Syndrome Complex BLOC-1 and its Cargo Phosphatidylinositol-4-kinase Type II Alpha. Molecular biology of the cell. 2013
38. Maxfield FR, McGraw TE. Endocytic recycling. Nat Rev Mol Cell Biol. 2004; 5:121–132. [PubMed: 15040445]
39. Pu J, Schindler C, Jia R, Jarnik M, Backlund P, Bonifacino JS. BORC, a multisubunit complex that regulates lysosome positioning. Dev Cell. 2015; 33:176–188. [PubMed: 25898167]
40. Setou M, Nakagawa T, Seog DH, Hirokawa N. Kinesin superfamily motor protein KIF17 and mLin-10 in NMDA receptor-containing vesicle transport. Science. 2000; 288:1796–1802. [PubMed: 10846156]
41. Matus A. Actin-based plasticity in dendritic spines. Science. 2000; 290:754–758. [PubMed: 11052932]
42. Idrissi FZ, Blasco A, Espinal A, Geli MI. Ultrastructural dynamics of proteins involved in endocytic budding. Proc Natl Acad Sci U S A. 2012; 109:E2587–2594. [PubMed: 22949647]
43. Kukulski W, Schorb M, Kaksonen M, Briggs JA. Plasma membrane reshaping during endocytosis is revealed by time-resolved electron tomography. Cell. 2012; 150:508–520. [PubMed: 22863005]
44. Monfregola J, Napolitano G, D'Urso M, Lappalainen P, Ursini MV. Functional characterization of Wiskott-Aldrich syndrome protein and scar homolog (WASH), a bi-modular nucleation-promoting factor able to interact with biogenesis of lysosome-related organelle subunit 2 (BLOS2) and gamma-tubulin. The Journal of biological chemistry. 2010; 285:16951–16957. [PubMed: 20308062]
45. Mayran N, Parton RG, Gruenberg J. Annexin II regulates multivesicular endosome biogenesis in the degradation pathway of animal cells. Embo J. 2003; 22:3242–3253. [PubMed: 12839987]
46. Morel E, Gruenberg J. The p11/S100A10 light chain of annexin A2 is dispensable for annexin A2 association to endosomes and functions in endosomal transport. PLoS One. 2007; 2:e1118. [PubMed: 17971878]

47. John Peter AT, Lachmann J, Rana M, Bunge M, Cabrera M, Ungermann C. The BLOC-1 complex promotes endosomal maturation by recruiting the Rab5 GTPase-activating protein Msb3. The Journal of cell biology. 2013; 201:97–111. [PubMed: 23547030]

48. Ryder PV, Faundez V. Schizophrenia: the “BLOC” may be in the endosomes. Sci Signal. 2009; 2:pe66. [PubMed: 19843956]

49. Heiligenstein X, Hurbain I, Delevoye C, Salamero J, Antony C, Raposo G. Step by step manipulation of the CryoCapsule with HPM high pressure freezers. Methods Cell Biol. 2014; 124:259–274. [PubMed: 25287845]

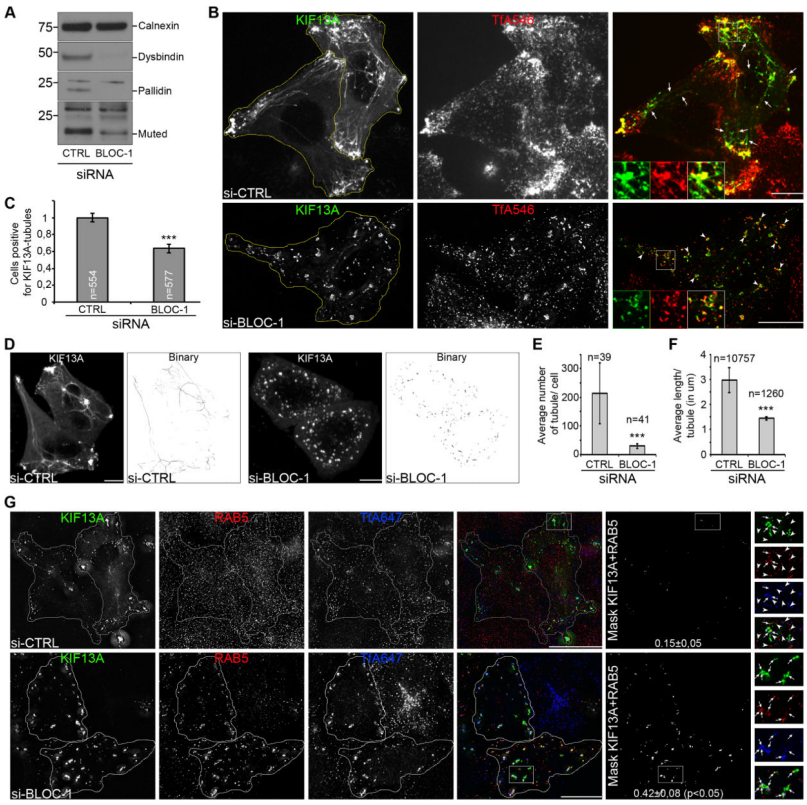

Figure 1. BLOC-1 is required to generate recycling endosome tubules (related to Supplemental Figure S1, Movies S1–S3)

(**A**) Western Blot (WB) of CTRL or BLOC-1 siRNAs-treated HeLa cell lysates probed with antibodies to Dysbindin, Pallidin, Muted or Calnexin. (**B**) Live imaging frames of KIF13A-YFP expressing siCTRL or siBLOC-1-treated cells that internalized TfA546. Arrows, $KIF13A^+$ tubules in siCTRL cells; arrowheads, KIF13A in $TfA546^+$ endosomes of siBLOC-1 cells (see Figure S1, Movies S1–S3). (**C**) Quantification of the percentage of n siCTRL or siBLOC-1 cells generating at least one $KIF13A^+$ tubule. (**D**) Maximum projections of 3D-stacks of live cell images of siCTRL or siBLOC-1-depleted cells and associated binary images after “skeletonize” processing. (**E**) Quantification of the average number of tubules per n siCTRL or siBLOC-1 cells. (**F**) Quantification of the average length (μm) per n tubules in siCTRL or siBLOC-1 cells. (**G**) siCTRL or siBLOC-1 cells expressing KIF13A that internalized TfA647 were analyzed by IFM after labeling for RAB5. Colocalization masks and Pearson’s coefficient are shown in the 5^{th} column. 6^{th} column, magnified boxed insets; arrows, codistribution of KIF13A with RAB5 and Tf in siBLOC-1 cells; arrowheads, lack of overlap in siCTRL cells. Data represent the average at least 4 independent experiments, normalized to control (**C**) and presented as a mean ± SD (see Supplemental Information). ***, $p<0.001$. Molecular masses in kD. Bars, 10 μm.

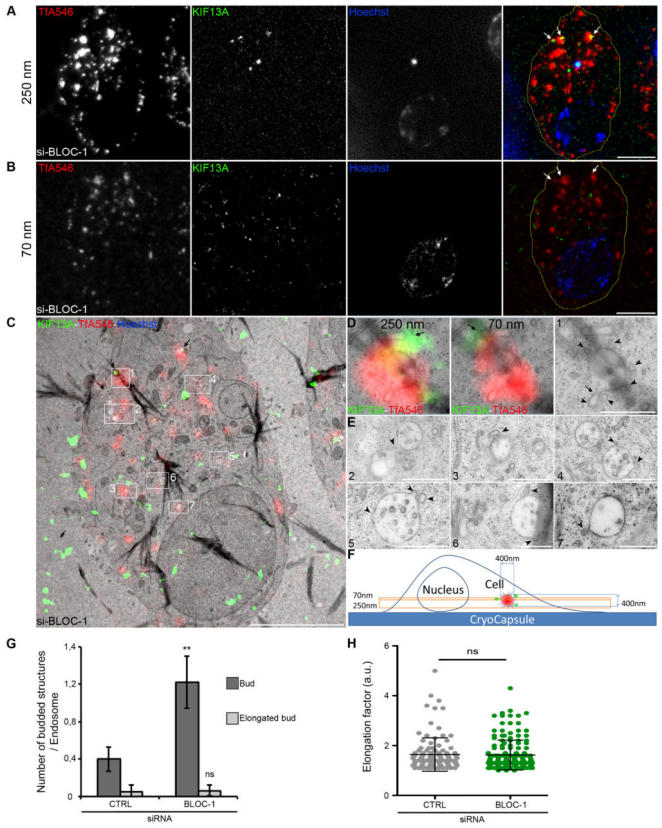

Figure 2. BLOC-1 promotes recycling endosome tubule elongation (related to Supplemental Figure S2, Movie S4)

(**A**) High pressure frozen siBLOC-1 HeLa cells analyzed by FM on the 250 nm thick section. Nucleus was stained with Hoechst (blue; bright dot, hole in the section). Arrows, large TfA546^{+} (red) and KIF13A^{+} (green) endosomes. (**B**) Same endocytic structures (arrows) identified by FM on the consecutive thin section (70 nm). KIF13A (YFP) signal was barely detected and post-processed to increase signal to noise ratio. (**C**) Overlay of the FM image (**B**) with the EM micrograph identifying the same endosomal structures (black arrows). White boxes, Tf^{+} and KIF13A^{+} structures (box 1, panels **D**) or Tf^{+} endosomes (boxes 2–7, panels **E**). Dark trails, folds in the section. (**D**) Magnified insets of boxed area (1) merging the FM images acquired on 250 nm (left) or 70 nm (middle) sections. KIF13A localization was shifted along an endosomal tubule nearby SE (arrows). EM micrograph (right) shows buds or vesicles (arrowheads) associated to vacuolar SE containing ILVs. Arrow, cross-section of an elongated bud with a tubular neck emanating from SE. (**E**) Magnified insets of boxed areas (2–7). Heavily (2–3) or faintly (4–7) TfA546^{+} endosomes corresponded to SEs harboring budded profiles (arrowheads). (**F**) Diagram of a cell grown on CryoCapsule® and of the thin and thick sections related to the size of fluorescent endosomes. Several budding profiles observed on thin section suggest that endosomal surface is covered by membrane deformations (see Movie S4). (**G**) Quantification of the number of bud and elongated bud structures on endosomes by CLEM. (**H**) Elongation factor of buds in siCTRL and siBLOC-1 cells. Data represent mean ± SD. ns: non significant; **, $p<0.01$. Scale bars, 5 μm (FM); 5 μm (EM, C); 500 nm (EM, DE).

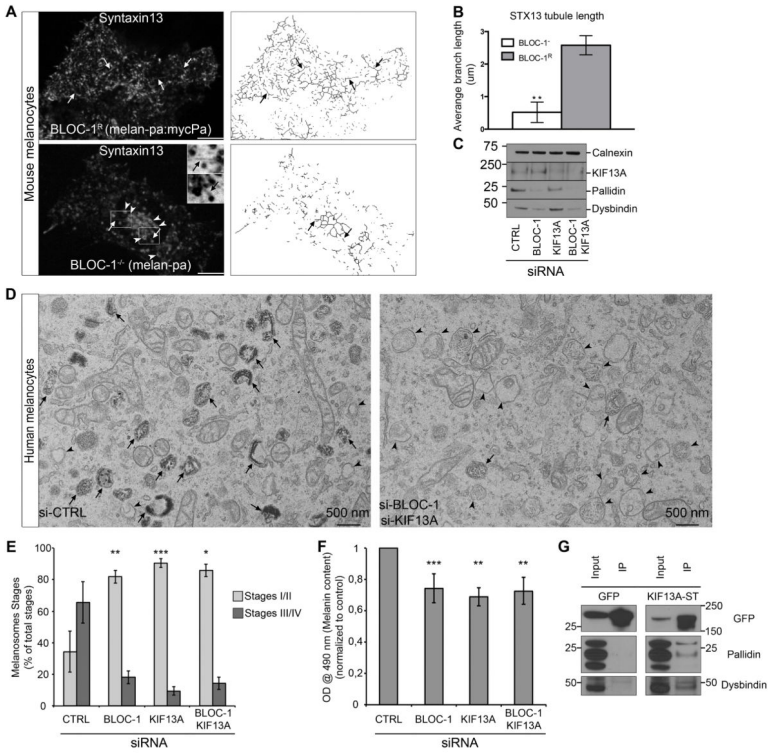

Figure 3. BLOC-1 and KIF13A cooperate for melanosomes biogenesis (related to Supplemental Figure S3)

(**A**) Live cell spinning disk confocal microscopy analysis of immortalized BLOC-1-deficient (BLOC-$1^{-/-}$; melan-pa1; bottom) or "rescued" (BLOC-1^{R}; melan-pa1:mycPa; top) mouse melanocytes expressing GFP-Syntaxin13 (STX13). Shown are individual frames before (left) or after "skeletonize" processing (right). Arrows, $STX13^{+}$ tubules; arrowheads, enlarged vacuolar endosomes in BLOC-$1^{-/-}$ cells. (**B**) STX13 tubule length was measured (mean ± SD) as the branch length in skeletonized frames. (**C**) WB of human MNT-1 melanocyte lysates depleted for either BLOC-1, KIF13A or both together. (**D**) Conventional EM analysis of siCTRL or siBLOC-1 and siKIF13A MNT-1 cells. Arrowheads, immature melanosomes; arrows, mature pigmented melanosomes. (**E**) Quantification of immature melanosomes (stages I/II) and mature melanosomes (stages III/IV) per condition. (**F**) Melanin content estimation of cells treated with CTRL, BLOC-1, KIF13A or both siRNAs. (**G**) WB of GFP immunoprecipitations (IP) of GFP- or GFP-KIF13A-ST-expressing HeLa cell lysates analyzed using GFP (top), Pallidin (middle) or Dysbindin (bottom) antibodies. Data represent the average of at least 3 independent experiments, normalized to control (**F**) and presented as a mean ± SD (see Supplemental Information). ***, $p<0.001$; **, $p<0.01$; *, $p<0.05$. Scale bars 10 µm (IFM), 500 nm (EM). Molecular masses in kD.

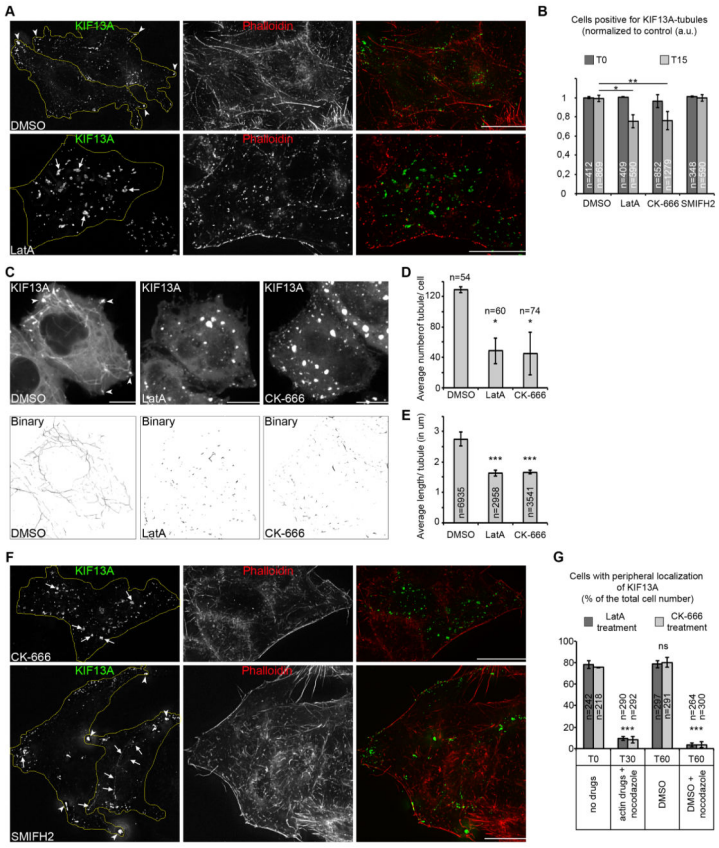

Figure 4. Actin dynamic and ARP2/3 stabilize recycling tubules (related to Supplemental Figure S4, Movie S5)

(**A**) IFM on DMSO- or LatA-treated, KIF13A expressing HeLa cells stained for F-actin (Phalloidin-A546). Arrows, KIF13A$^+$ vesicular structures; arrowheads, KIF13A at cell periphery. (**B**) Quantification of the percentage of DMSO-, LatA-, CK-666- or SMIFH2-treated cells generating at least one KIF13A$^+$ tubule. (**C**) Maximum projections of 3D-stacks of live cell images of DMSO-, LatA- or CK-666-treated KIF13A expressing cells and associated binary images (skeletonize). Arrowheads, KIF13A$^+$ structures at cell periphery. (**D**) Quantification of the average number of tubules per n cells treated in C. (**E**) Quantification of the average length (in µm) per n tubules in cells treated in C. (**F**) IFM on CK666- or SMIFH2-treated, KIF13A expressing HeLa cells stained for F-actin (Phalloidin-A546). Arrows, KIF13A$^+$ vesicular structures; arrowheads, KIF13A at cell periphery. (**G**) Percentage of n cells with peripheral KIF13A$^+$ structures fixed before (T0), after (T30, actin drugs+nocodazole) 30 min incubation with LatA (dark grey bars) or CK-666 (light grey bars) with nocodazole, then after DMSO (30 min, T60 DMSO) or DMSO + nocodazole (30 min, T60 DMSO+nocodazole). Data are presented as the average of two to four independent experiments, normalized to control (**B**) and presented as a mean ± SD. *, $p<0.05$; **, $p<0.01$; ***, $p<0.001$. Scale Bars, 10 µm (IFM).

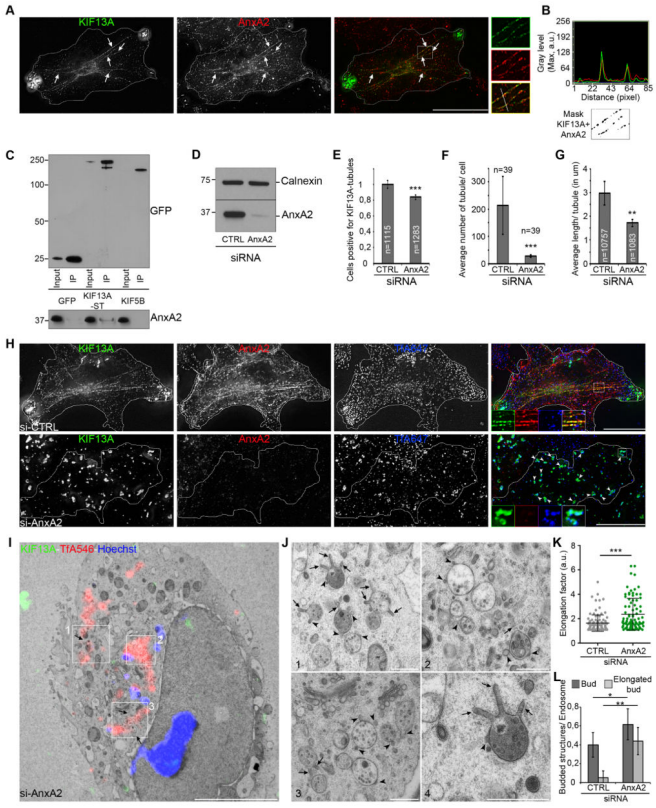

Figure 5. Annexin A2 and KIF13A cooperate for recycling tubules formation (related to Supplemental Figure S5, Movie S6)

(**A**) IFM of KIF13A-expressing (green) HeLa cells labeled with AnxA2 (red) antibody. Arrows, KIF13A$^+$ and AnxA2$^+$ RE tubules. (**B**) Intensity profile of KIF13A (green) and AnxA2 (red) fluorescence along tubules (white line in A, merged panel box). Co-localization mask (bottom) of KIF13A$^+$ and AnxA2$^+$ pixels from the merged panel inset. (**C**) WB of IP of GFP, GFP-KIF13A-ST or YFP-KIF5B expressing HeLa cells lysates analyzed using GFP (top) or AnxA2 (bottom) antibodies. (**D**) WB of si-CTRL- or si-AnxA2 HeLa cells lysates using AnxA2 or calnexin antibodies. (**E**) Quantification of n siCTRL or siAnxA2 cells generating at least one KIF13A$^+$ tubule. (**F**) Quantification of the average number of tubules per n siCTRL or siAnxA2 cells. (**G**) Quantification of the average length (in μm) per n tubules of siCTRL or siAnxA2 cells. (**H**) IFM of siCTRL or siAnxA2, KIF13A (green) expressing HeLa cells labeled for AnxA2 (red) antibody that internalized TfA647 (blue). Arrowheads, KIF13A in Tf$^+$ vesicular endosomal structures. Magnified insets (boxed areas) of singles and merged panels are shown. (**I**) CLEM on AnxA2-depleted Hela cells expressing KIF13A that internalized TfA546. FM image on 70 nm section (see Figure S5F) overlaid to the EM micrograph. Arrows, correlated Tf$^+$ and KIF13A$^+$ structures (see Figure S5E–F); white boxes, Tf$^+$ and KIF13A$^+$ structures. (**J**) Magnified insets (boxed areas) of SEs containing ILVs harboring buds (arrowheads) or elongated budding structures (arrows) in continuity with vacuolar domains (see Movie S6). (**K**) Elongation factor of buds in siCTRL and siAnxa2 cells. (**L**) Quantification of the number of bud and elongated bud structures on endosomes in siCTRL and siAnxa2 cells. Data are presented as a mean ± SD. Others represent the average of 3 independent experiments, normalized (**E**) to control and

presented as a mean ± SD. *, $p<0.05$; **, $p<0.01$; ***, $p<0.001$. Molecular masses in kD. Scale bars, 10 μm (IFM); 5 μm (EM, G); 500 nm (EM, H).

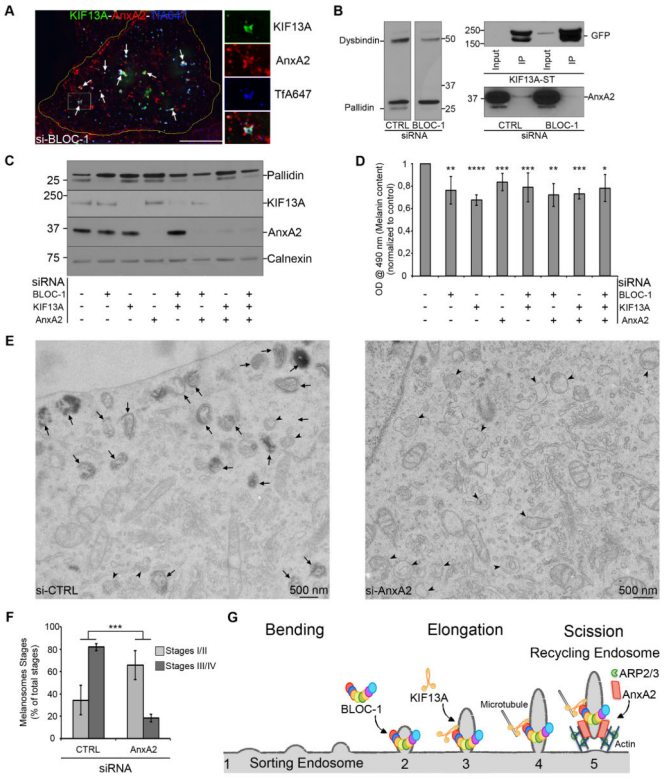

Figure 6. Annexin A2, BLOC-1 and KIF13A cooperate for melanosomes biogenesis (related to Supplemental Figure S6)

(**A**) IFM of AnxA2 (red) on KIF13A (green)-expressing siBLOC-1 HeLa cells that internalized TfA647 (blue). Arrows, triple KIF13A, AnxA2 and Tf^{+} endosomes. (**B**) WB representative of 3 independent IPs of GFP-KIF13A-ST expressing siCTRL or siBLOC-1 HeLa cells lysates (left) analyzed using GFP (top right) or AnxA2 (bottom right) antibodies. Lower AnxA2 amount is revealed in siBLOC-1 IP while greater KIF13A-ST was immunoprecipitated relative to controls. (**C**) WB of siRNAs treated MNT1 lysates using pallidin (top), KIF13A (middle top), AnxA2 (middle bottom) or calnexin (bottom) antibodies. (**D**) Intracellular melanin quantification of MNT1 cells as in **C**. (**E**) Conventional EM analysis of siCTRL or siAnxA2 MNT1 cells. Arrowheads, immature melanosomes stages I/II; arrows, mature pigmented melanosomes stages III/IV. (**F**) Quantification of melanosomes stages in siCTRL or siAnxA2 MNT1 cells. (**G**) Model of recycling endosomes shaping by BLOC-1. BLOC-1 binds to highly curved SE membrane deformations (**1**–**2**). KIF13A interacts with BLOC-1 at the newly formed tubule (**3**) and generates the pulling force to elongate the RE tubule from SE (**4**). AnxA2 binds to SE elongated bud, promotes the ARP2/3-dependent polymerization of branched actin filaments and participates to the stabilization and/or scission of RE tubules (**5**). Data represent the average of at least 3 independent experiments, normalized to control and presented as a mean ± SD. Scale bars: 500 nm (EM); 10 μm (IFM). ****, $p<0.001$; ***, $p<0.01$; **, $p<0.02$; *, $p<0.05$.